

CRACK NUCLEATION AND PROPAGATION IN HIGH STRENGTH WELDED PIPES

I.Yu. Pyshmintsev¹, A.O. Struin¹, V.N. Lozovoy¹, A. B. Arabey², T.S. Esiev³

¹ RosNITI (The Russian Research Institute of the Tube and Pipe Industry);
30 Novorossiyskaya str.; Chelyabinsk, 454139, Russia

² GAZPROM; 16 Nametkina str.; Moscow, 117997, Russia

³ GAZPROM VNIIGAZ; Razvilka settl.; Moscow region, 142717, Russia

Keywords: Weld Joint of X70, X80 Linepipe, Hydraulic and Pneumatic Tests, Nucleation and Crack Propagation, Spiral Pipes

Abstract

The effect of local embrittlement of the weld joint on the structural strength of high-strength pipe is discussed in the paper. The results of hydraulic tests of X70 grade pipes having a longitudinal surface notch in the base metal and weld joint are presented. By using examples of full-scale burst tests, features of ductile fracture propagation in spiral pipes are displayed.

Introduction

For economic reasons, there is a growing production of large diameter pipe manufactured from microalloyed steel of X70 Grade (according to the American Petroleum Institute classification) or higher [1]. Modern metallurgical, rolling, and welding technologies have resulted in high plasticity and low temperature toughness of the base metal (BM). Stricter requirements on the properties of the weld are the result of the improved properties of the base metal. It is obvious that the weld joint is still considered as the most critical part with potentially low toughness properties where cracks can nucleate and then propagate.

It is important to develop requirements for high-strength pipe, including theoretically derived and experimentally confirmed values of weld joint toughness. Recent practice calls for determination of the impact toughness in the weld seam (WS) and the heat affected zone (HAZ), including the fusion line, in samples with a V-notch. The requirements for toughness of weld joints at -20 and -40 °C, for recent gas pipeline projects, are remarkably high, although significantly lower than for the base metal. As an example, Table I and Figure 1 present the Charpy requirements for the BM and weld joints in high-strength pipes (diameter 1220–1420 mm) according to the ISO 3183:2007/API Spec 5L standard [2]. The minimum values for the recent Bovananokovo–Ukhta (from the Yamal peninsula) gas pipeline and the VSTO oil pipeline (between Eastern Siberia and the Pacific Ocean) are also presented.

Table I. Minimum Average Charpy Energy for Base Metal and Weld Joint in High-Strength Pipes

Specification	Grade pipes	Temperature, °C	Absorbed Charpy energy, Joules/cm ²	
			Base metal	Weld
ISO 3183:2007	X70	0	68	50
VSTO pipeline	X70	-10	79	39
Bovanenkovo-Ukhta pipeline	X70	-40	170*	53
	X80	-40	250	70

*test at minus 20 °C

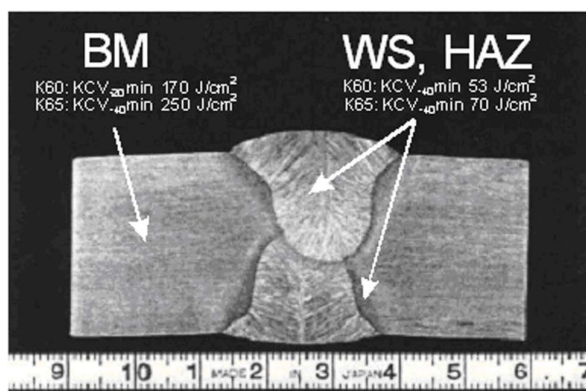


Figure 1. Weld joint of X70 grade pipe.

The influence of local embrittlement in the HAZ on the structural strength, or burst pressure, of high-strength pipe, remains controversial [3, 4]. It is likely that relatively low toughness of the welds, when defects nucleate, may lead to premature (brittle) failure of the pipe. To assess the influence of local brittleness in the weld joint on the structural strength of high-strength pipe, it is necessary to use full scale experiments.

Hydraulic Tests

Hydraulic tests of pre-notched, full-size, longitudinally welded pipes corresponding to X70 Grade have been conducted. Four sizes were tested: 530 x 18.9 mm, 1020 x 29.8 mm, 1220 x 17.8 mm, and 1420 x 25.8 mm. The length of the test pipe was at least three diameters. To assess the influence of a weld joint on the reliability of pipe with a sharp surface defect, five positions were used over the pipe perimeter: 90° from the weld; 100 mm from the fusion line (FL); 50 mm from FL; and in the HAZ, with the tip of the notch directly at the FL and at the center of the seam weld (SW). The position of the notch in the weld was evaluated using transverse sections before and after testing. The notch was machined by a V-shape miller (diameter 125 mm, thickness 2.5 mm) with a vertex angle of $60 \pm 5^\circ$ and with radius of 0.1 mm at the tip. The

depth/length ratio of the notch was selected so that the calculated burst pressure for a pipe with a longitudinal defect corresponds to the maximum test pressure for the gas pipeline where the pipe is to be used.

The tests were conducted at -20 ± 2 °C. The pipe around the notch (length 2.0 m; width 0.5 m) was cooled by liquid nitrogen and added to a heat insulated bath installed on the outer upper surface. To ensure uniform temperature through the wall, the inner surface of the pipe was insulated. The hydraulic test bench is shown in Figure 2. Burst pressure and the crack size were measured.

Charpy energy, static toughness, and strength of the BM and weld were determined in accordance with the GOST 9454–78, BS 7448:2005 (parts 1 and 2), GOST 1497–84, and GOST 6996–66 standards, respectively. Table II presents the strength of tested pipes.

The static toughness was measured on full thickness samples with an edge crack, in three point bending (SENB sample [5, 6]) at -20 ± 2 °C. Critical values of stress intensity factor (K_Q in the standard [5]) and crack tip opening displacement (CTOD) were measured. The fracture in SENB samples and corresponding curves are shown in Figure 3. Table III presents the test results for samples from the 1220 x 17.8 mm pipe.

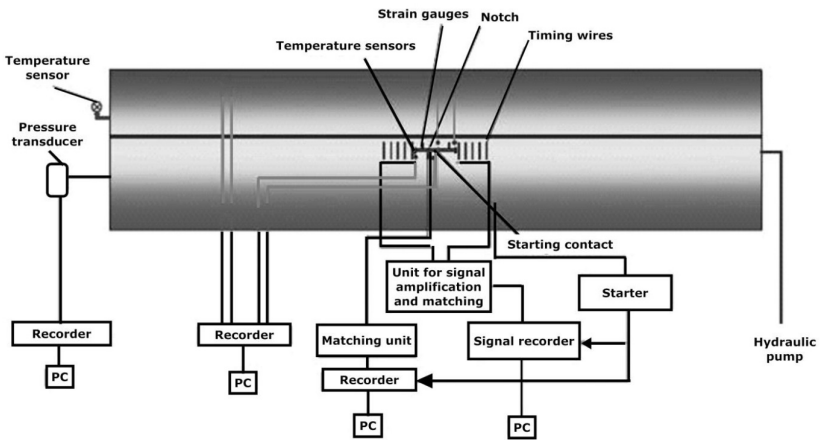


Figure 2. Hydraulic test schematic.

Table II. Strength of Pipes

Pipe sizes mm	Tensile strength, MPa		
	BM	FL	SW
530 x 18.9	640	654	652
1020 x 29.8	642	695	698
1220 x 17.8	647-668	652-657	647-661
1420 x 25.8	644	668	678

Table III. Stress Intensity Factors and CTOD for Transverse Samples for 1220x17.8 mm pipe

Sampling	K_Q , MPa m ^{0.5}	CTOD, mm
Base metal	1545	1.15
	2150	1.09
	1950	1.21
Fusion line	2870	0.193
	2615	0.212
	2425	0.189
Weld seam (WS)	2565	0.191
	2685	0.139
	2598	0.225

The tests show that K_Q is smaller for the BM than for the weld joint. The difference is around 28 percent. CTOD is considerably greater in the base metal: 1.150 mm, on average, as against 0.198 and 0.185 mm for the FL and the center of the weld seam, respectively.

Significant differences between the fractures of the BM and the weld were found. The fracture surface in the BM is uniform and typical for ductile fracture, Figure 3. The fracture surfaces in HAZ (FL) and in the center of the SW correspond to brittle failure.

Table IV presents the results of 23 hydraulic tests for 530 x 18.9 mm, 1220 x 17.8 mm, 1020 x 29.8 mm, and 1420 x 25.8 mm pipes with machined sharp surface defects. It is evident, Figure 4, that the observed leak-to-break transition for all notch positions occurs when the notch length is increased from 265 to 308 mm. Thus, this transition from flaw (leak) to crack propagation is not sensitive to lower CTOD of the FL or WS.

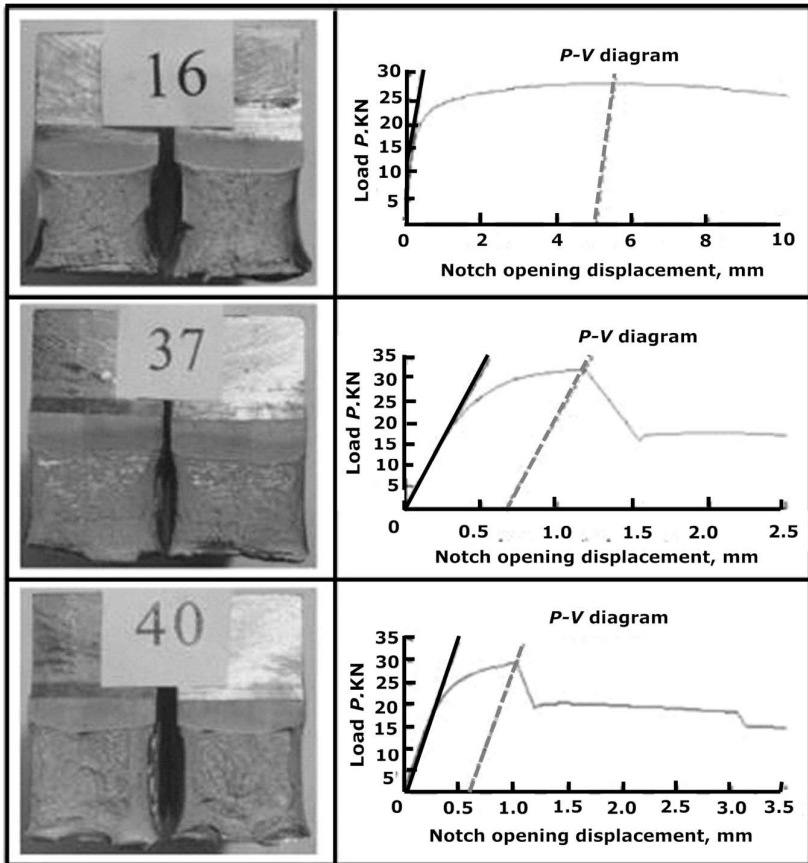


Figure 3. Fractures of SENB samples and corresponding loading diagrams. Top – base metal. Centre – weld seam. Bottom – fusion line.

The longest cracks are found in the weld joint when the pipe is notched on the FL and in the center of the SW, Figure 4. If the notch is machined in the center of the SW, the crack begins to propagate along and then passes to the fusion line - that is, to the zone of local brittleness - and moves along that line until stopped, Figure 5. If the length of notch in the weld joint is long for crack propagation the fracture stops only at the boundary of the cooling zone - in other words, crack arrest occurs on account of the sharp increase in metal temperature, and thus notch toughness.

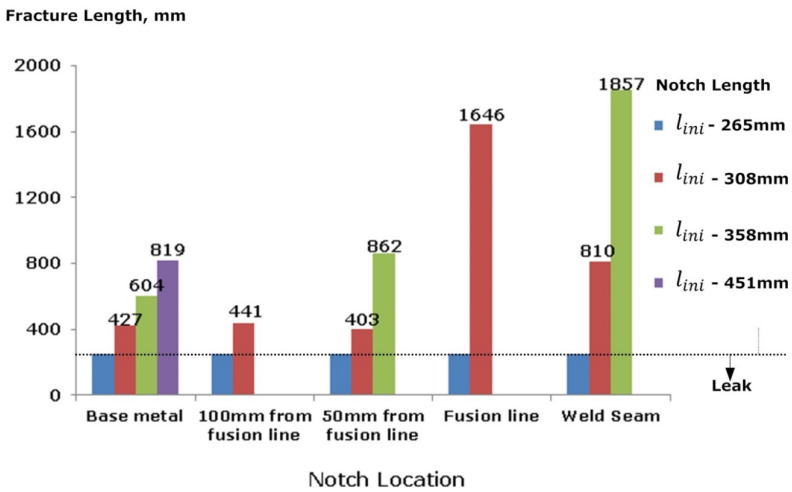


Figure 4. Fracture length in tests.

Table IV. Hydraulic Test Data

№	Notch position	Wall thickness, mm	Notch length, mm	Notch depth, mm	Burst pressure, MPa	Full crack length, mm
OD = 530 mm, WT = 18.9 mm						
1	BM	19.0	360	14.0	18.8	360
2	FL	19.4	306	14.4	18.7	1167
3	SW	21.0	307	16.2	18.5	690
OD = 1020 mm, WT = 29.8 mm						
4	BM	29.8	548	20.6	17.3	633
5	FL	30.3	335	25.0	18.3	335
6	SW	30.9	334	26.1	19.5	334
OD = 1220 mm, WT = 17.8 mm						
7	BM	17.9	265	14.0	10.2	265
8		17.8	308	11.9	11.6	427
9		17.8	358	11.3	10.6	604
10		17.8	451	10.5	10.7	819
11	50 mm from FL	17.9	266	13.7	10.9	266
12		17.8	308	11.9	11.4	403
13		17.8	358	11.5	11.6	862
14	100 mm from FL	17.6	265	13.2	11.5	265
15		17.6	308	11.7	11.0	441
16	FL	18.4	268	14.1	10.2	268
17		18.8	308	13.0	11.4	1646
18	SW	18.4	265	14.2	10.0	265
19		18.5	308	12.4	11.3	810
20		18.7	358	12.6	10.7	1857
OD = 1020 mm, WT = 29.8 mm						
21	BM	25.8	294	21.9	12.5	280
22	FL	26.1	240	23.3	14.5	228
23	SW	25.7	240	22.6	14.8	220

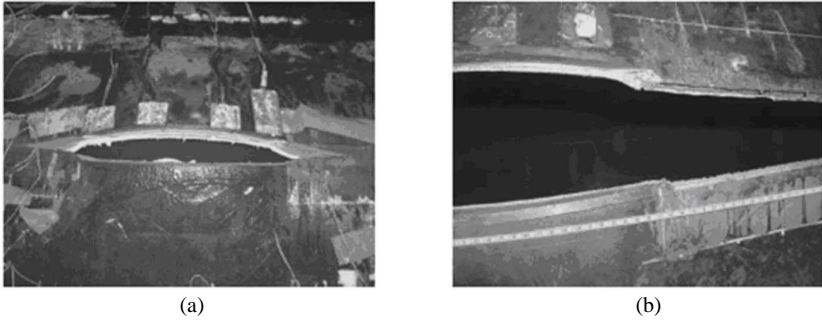


Figure 5. Pipe fracture as a function of notch location: (a) notch in base metal ($l = 308$ mm); (b) notch at center of the weld seam ($l = 358$ mm).

The hydraulic test data are evaluated by two fundamentally different approaches. The first is based on hydraulic test parameters. The burst pressure, P (MPa), in a pipe with a defect is calculated using a known formula based on tensile strength and Folias correction [3, 4]

$$P = \frac{2\sigma_{ss}}{\left(\frac{D}{t} - 1\right)} \cdot \left(\frac{1 - \frac{d}{t}}{1 - \frac{d}{t \cdot M_F}} \right) \quad (1)$$

where σ_{ss} is tensile strength, MPa;

D is the external pipe diameter, mm; t is the pipe's wall thickness, mm;

d is the defect depth, mm;

M_F is the correction factor (Folias coefficient [7]).

The need for M_F arises in that the edge of the crack bends outward under the action of the internal pressure. For the pipe here considered [3], R is outer pipe radius, L is defect length.

$$M_F = \sqrt{1 + 0.31(L/\sqrt{2Rt})^2} \quad (2)$$

Calculations using Equations (1) and (2) show that, if the depth of the cut is less than 80% of the pipe's wall thickness, the calculated burst pressure differs from the actual value by less than 10%, Figure 6. Thus, burst pressure is controlled by tensile strength of base metal rather than toughness.

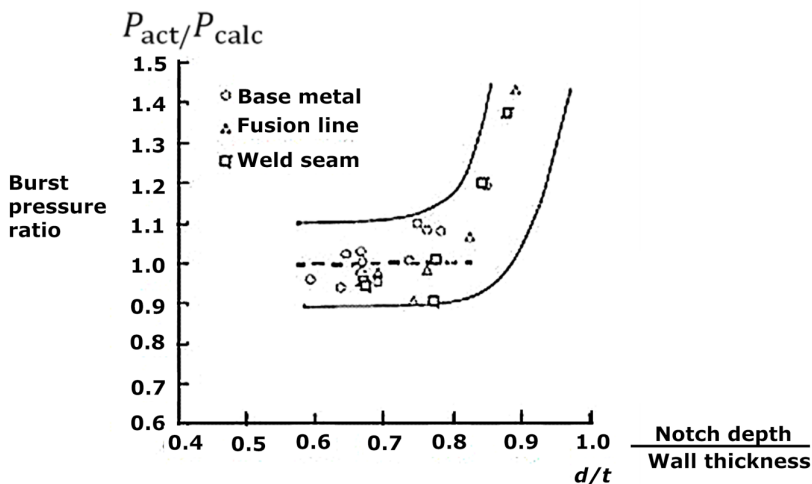


Figure 6. Deviation of measured burst pressure from the values given by Equations (1) and (2).

The second approach, based on failure mechanics and the failure assessment diagram (FAD), is regulated by the BS 7910:2005 standard [8]. The FAD diagram is plotted using the formula:

$$K_r = S_r \left(\frac{8}{\pi^2} \ln \sec \left(\frac{\pi}{2} S_r \right) \right)^{-0.5} \quad (3)$$

K_r is ratio of stress intensity factor for mode I to effective stress intensity factor, S_r is ratio of applied stress to collapse stress of the structure. The second approach, which draws on known principles of elastoplastic fracture mechanics, is associated with several indeterminacies.

For correct calculation, we need to know the stress intensity coefficient of the structure (K calibration). In shell theory, through-wall defects of different shape and orientation are mainly considered. Surface defects, as a rule, are represented as half of an ellipse, whose length is no more than twice the thickness. Appropriate K calibration remains to be completed for the given case. For a pipe with surface defects whose length exceeds the depth by at least two orders of magnitude, K calibration requires additional work.

It has been shown experimentally, Table II, that the forces corresponding to the failure strength in the zones of local brittleness are relatively high and do not differ greatly from those in the base metal, despite the significant difference in the critical plastic or fracture characteristics. Accordingly, it is incorrect to use the critical opening at the crack tip on the basis of Equation (3), as was done in the past [3, 4]. This approach yields an anomalously low fracture pressure, which is not confirmed in practice or by the given tests.

Hydraulic tests yield important results regarding zones of local brittleness within the weld joint and their role in failure. It is obvious that pipe failure occurs at practically the same internal pressure, regardless of the defect location. This means that the conditions of crack initiation in the BM and the weld joint (SW or FL) may reasonably be regarded as similar. However, the length of propagation for a crack formed in the BM and the weld joint will be fundamentally different.

It can be assumed that the crack initiation in the BM and the weld joint is determined by the overall strength of the pipe controlled by BM tensile strength. The initiation of failure is probably due to the onset of macroplastic deformation in the middle of the cut, on account of high local deformation. This is also possible when the notch is in the weld joint, since fracture toughness tests show the presence of relatively high plastic deformation preceding brittle crack propagation in the weld joint. Nevertheless, crack propagation is ductile in the base metal or predominantly brittle in the weld joint, depending on the ductility of the metal in the vicinity of the notch.

Crack propagation is determined by the accompanying plastic strain (absorbed energy) [9]. In brittle failure of the weld, the crack length is clearly higher than in the ductile base metal, Figures 4 and 5. It is apparent that zones of local brittleness in the weld joint impair the pipe's structural strength in terms of resistance to crack propagation. Hydraulic tests of X70 1220 x 17.8 mm pipes showed a critical crack length between 265 and 308 mm. No difference in critical crack length in the base metal and weld joint was found; this may be attributed to the distinguishing features of failure in pipe with a surface defect. After failure, the metal layer under the notch tip is transformed into a defect through the entire wall, whose initiation depends on the strength properties of the pipe. For crack propagation after the formation of such a defect, crack nucleation at defect ends is required. This occurs with the given properties of the pipe as a result of macro plastic deformation. Since the weld softened zone is characterized by minimum strength, the plastic strain is concentrated there and accompanied by ductile crack growth. This is observed in tests of 1220 x 17.8 mm pipe with FL notch length 265 mm, Figure 7. The crack rapidly stops in the BM in this case.

Pneumatic Test



Figure 7. Point at which crack stops in pipe with a diameter of 1220 mm and wall thickness of 17.8 mm fusion line notch location.

Technical progress in steel making and pipe making has allowed the achievement of better strength and low temperature behavior of both the base steel and weld joint, which has resulted in an increased working pressure in trunk gas pipelines [10]. It formed the basis for further improvement in strength-ductility combinations and for the development of new steel grades with strength higher than the widely used X70. Attempts to expand acknowledged approaches to predict the required arrest toughness for the new generation of pipelines cannot be characterized as successful. One of the most important issues for new higher pressure pipelines is the development of appropriate fracture control strategies and design against ductile fracture propagation. Traditionally, fracture control has been accomplished by selecting pipe materials which behave in a ductile manner at the required operating temperature and are capable of arresting a propagating fracture, if initiated. The Charpy absorbed energy needed for arrest is established based upon the actual absorbed energy of the pipe in which arrest is observed to occur in full scale pneumatic tests [11-15].

This study is devoted to analysis of full scale burst tests of 1420 x 21.6 mm longitudinally and spiral welded X70 pipes developed for 9.8 MPa gas pressure. The arrestability under severe climatic conditions can be evaluated using a standard approach based on measurements and calculations of Charpy energy at low temperature and comparisons of additional data collected during pipe section burst testing and mechanical tests of steels. Being dependent on microstructure, the mechanical behavior of the base metal and the weld shall be considered and compared with ductile fracture behavior of tested traditional steels with ferrite-pearlite (FP) microstructures and steels with complex multiphase, predominantly acicular ferrite (AF), microstructures developed in the past decades. The second type of steel can be considered as advanced due to more uniform and finer microstructure and consequently better ductility [10]. While generally this test is applied to evaluate arrestability of the base metal, a main feature of spiral welded pipe is the single or periodical interaction of the crack and seam weld.

Three spiral welded (SW) and three longitudinally welded (LW) pipes were installed in test sections constructed on both sides of a 6m initiating pipe. The total length of the test line with buffer sections was 165 m.

The chemical compositions of the TMCP (Thermo Mechanically Processed) steels are given in the Table V. Optical and scanning electron microscopy revealed a fine grained slightly banded FP (ferrite/pearlite) microstructure with low pearlite fraction in the base metal of LW pipes. This microstructure is typical for plates subjected to traditional controlled rolling and accelerated cooling. Base metal microstructures in SW pipes are more complex but uniform containing fine ferrite grains, acicular ferrite and bainite. Details of these microstructures are difficult to resolve using optical microscopy due to the small sizes of all microconstituents. This type of microstructure is typical for modern lower carbon steels alloyed with elements increasing the stability of heavily deformed austenite and subjected to TMCP using high cooling rates after finish rolling. Lower carbon content and increased manganese concentration facilitate formation of a fine microstructure called generally AF (acicular ferrite) due to the predominance of acicular and lath microconstituents recognizable by optical microscopy. Typical microstructures of base metal are given in Figure 8.

Table V. Chemical Composition of Tested Steels

	Content of elements. wt %							
	C	Mn	Si	Nb	V	Ti	Al	N
LW	0.098	1.62	0.43	0.050	0.002	0.022	0.033	0.0036
SW	0.056	1.91	0.32	0.056	0.003	0.014	0.027	0.005
	S	P	Cr	Ni	Cu		Ceq	Pcm
LW	0.0008	0.011	0.024	0.046	0.029		0.40	0.20
SW	0.0005	0.009	0.17	0.013	0.012		0.43	0.17

Mechanical tests of transverse specimens showed high strength, ductility and low temperature toughness for both steels and weldments. The Charpy energy of the AF steel at -20 °C is about two times higher than for the FP steel but both steels have demonstrated fully ductile behavior below -40 °C. The main mechanical properties are presented in Table VI.

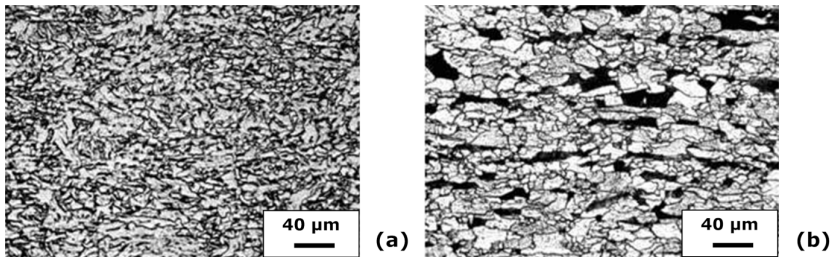


Figure 8. Optical micrographs of base metal in SW (a) and LW (b) pipes.

Table VI. Mechanical Properties of Tested Pipes

	Base metal			
	Yield stress, MPa	Tensile strength, MPa	El ₅ , %	Charpy energy at -20 °C (min), J/cm ²
LW	527/-	653/-	20.5/-	164
SW	540/505	655/650	24/24	338
	Weld joint			
	Absorbed energy, Joules/cm ² LW – test temperature minus 40 °(C) SW – test temperature minus 20 °(C)			
	Center line	Fusion line (FL)	FL+2mm	
LW	(171-186)/176	(171-213)/203	–	
SW	(65-90)/81	(178-200)/187	(258-326)/295	

Note- Tensile properties are given for flattened/round bar specimens; Charpy energies are given as scatter/mean values.

A crack initiated by explosion crossed girth welds and propagated into test pipes. On the longitudinal pipe side the fracture was arrested in 6.5 m. Along the spiral pipe the fracture propagated straight for 1.4 m and hit a spiral weld and then deviated to a helical path travelling along the fusion line of the spiral weld for about 1.6 m in the vicinity of the HAZ. The crack along the spiral weld reached the girth weld between the first and second pipes where it was stopped. Macro and microstructures of the base metal in a cross-section of the plastic strained zones, close to fracture surfaces, are presented in Figures 9 and 10.

Studies of the fracture surfaces have shown deep plastic straining, Figure 9a, as well as a long plastic zone in the circumferential direction in the base metal with the AF microstructure. No separations were found on the fracture surface in the base metal of SW pipes. Low plastic straining accompanied crack propagation in the steel with a FP microstructure, Figure 9b. Multiple separations on the fracture surface were seen along the total propagation length. Deflection to the helical path led to elimination of a visible plastic zone near fracture. Even in regions where the crack propagated in the HAZ and in base metal adjacent to the HAZ, very little localized strain was seen, Figure 9c. The fracture surface was at the plane close to 45 degree to the wall. Thus, the unwrapping along the weld led to transition to predominately plain shear fracture. Microfractography using scanning electron microscopy revealed fine elongated dimples typical for shearing. It is clearly seen that micro void nucleation in this area is predominantly located on ferrite-pearlite boundaries, Figure 10. The total density (volume fraction) of resolved voids is very low. Some voids were found in pearlite where, more likely, ductile shear crack nucleates as the leading process followed by separation along ferrite-pearlite boundaries.

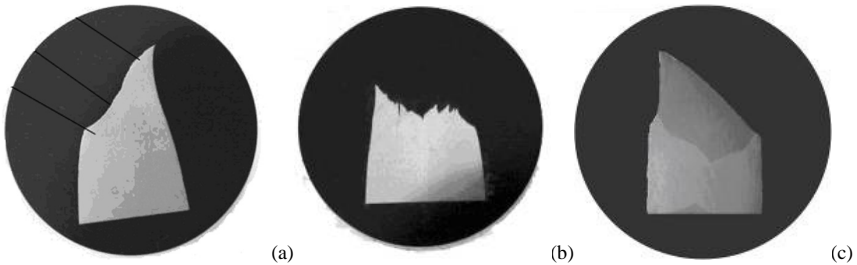


Figure 9. Cross section of base metal (a), (b) and in vicinity of spiral weld (c).
(a) – AF steel, (b) – FP steel.

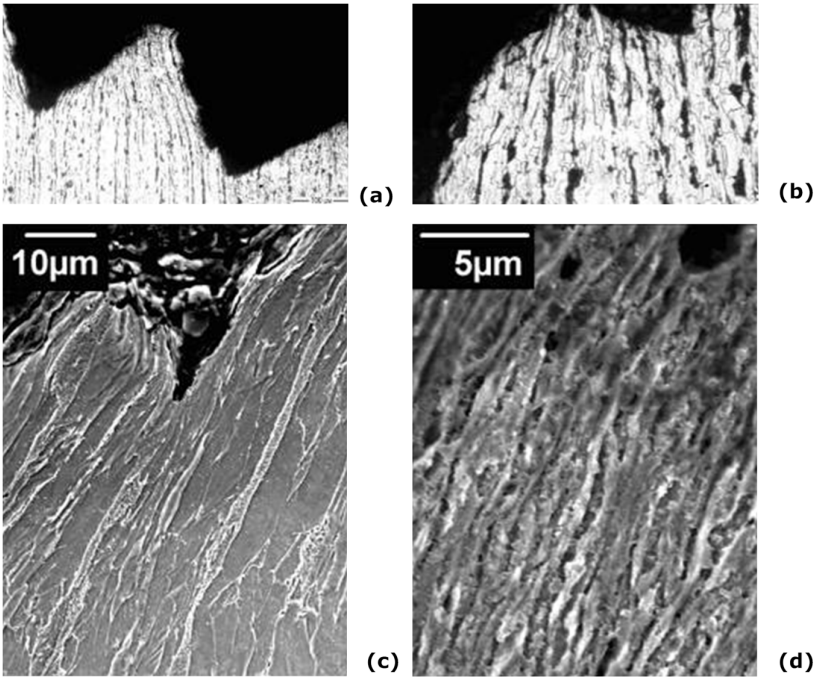


Figure 10. Fracture in base metal with FP microstructures in LW pipes (a) – (c) and fracture in AF microstructure in SW pipes (d) showing void formation.

A higher volume fraction of voids was found in the heavily strained AF microstructure. Voids are distributed very uniformly. Probably this is a result of a higher maximum strain before fracture and more uniform microstructure composed of constituents with almost equal strength, hardness and strain hardening behaviour.

Experiments have shown more ductile behavior of the AF microstructure in full scale burst tests which is in good correlation with almost two times higher Charpy energy than in steel with the same strength and a FP microstructure. Nevertheless since loading, sample thickness and crack speed are different in Charpy and in full scale arrest tests it is important to compare specific energies of propagation for these typical X70 microstructures.

Energies absorbed during plastic deformation of the steel were calculated based on strain hardening curves and measurements of plastic strain of pipe wall along the crack route. The plane strain ($\epsilon_2=0$) approach was used for strain calculations [10]:

$$e = \ln\left(\frac{t_o}{t}\right), \quad (4)$$

where t_0 , t – initial and current wall thicknesses .

Stress - strain curves for uniform and localized deformation were approximated from tensile tests and used for calculation of the energy of plastic deformation as:

$$S = 450 + 1415e^{0.651} \text{ for AF steel and } S = 480 + 995e^{0.516} \text{ for FP steel} \quad (5)$$

And

$$E = 2 \int_0^e S(e) \cdot V(e) de \quad (6)$$

S is true stress, V is volume of plastic deformation. Strain distribution along the hoop direction for AF and FP steels are presented in Figure 11. The strain hardening rate for the AF microstructure is remarkably higher than in the FP steel but it leads to a significant difference in maximum stresses at full scale fracture strains. However, higher stress combined with deeper straining and consequently increased volume of strained steel resulted in sufficient growth of absorbed energy, Figure 12. Absorbed energy in the FP steel was almost constant along the crack length but its value was about five times lower than in the steel with an AF microstructure while Charpy energies differed only by a factor of two.

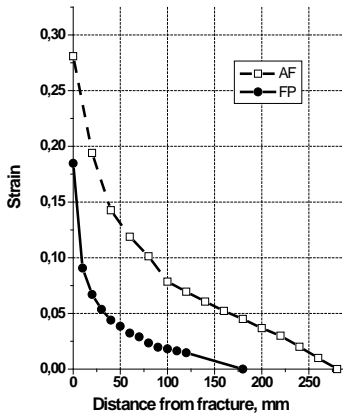


Figure 11. Strain distribution in hoop direction.

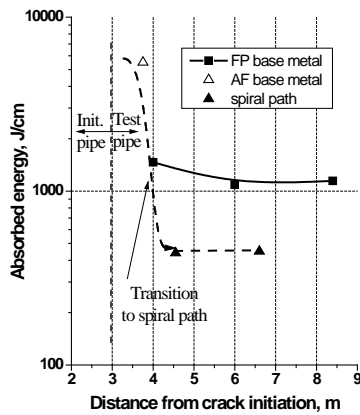


Figure 12. Absorbed energy versus crack length in tested pipes.

Deviation of the crack to a helical path along the spiral weld seam can be considered as the most favourable from an energy balance point of view, in spite of the increase in total crack length.

Probably retardation of plastic strain and stress concentration in the vicinity of the weld are main factors determining absorbed energy per unit crack length.

Conclusion

In spite of local brittleness in the weld joint, in comparison with base metal, the burst pressure of pre-notched high strength X70 pipes remains high and controlled by the strength of the pipe body. Crack nucleation at such a narrow sharp defect is mainly determined by the strength properties of the base metal, regardless of the notch position. A strong effect of defect position and local toughness on critical crack length was not found. However, hydraulic tests have revealed that crack propagation length is determined by the local properties of the weld joint. Arrest of running fracture in a gas pipeline, if it initiated in the weld, will be controlled by base metal straining energy in the next longitudinally welded pipe. Crack propagation along the spiral weld is caused by suppression of plastic strain in this area and transition from distributed straining with deep reduction to plain shear. To obtain better arrest behavior of spiral welded pipes at high pressure the optimization of weld design is required.

Acknowledgments

The authors gratefully acknowledge the support of GAZPROM, TMK and Volzhsky Pipe Plant. The authors wish to express their thanks to all colleagues from GAZPROM VNIIGAZ and RosNITI, who took part in discussions and experimental work.

References

1. I. Yu. Pyshmintsev, V.N. Lozovoi, and A.O. Struin, "Problems and Solutions Application X80 Grade Pipes," *Science and Engineering of Gas Industry*, 1 (2009), 22–29.
2. ISO 3183:2007/API Spec 5L Standard. Petroleum and Natural Gas Industries: Steel Pipe for Pipeline Transportation Systems, 2007.
3. B. Fu., et al., "Significance of Low Toughness in the Seam Weld HAZ of a 42-Inch Diameter Grade X70 DSAW Line Pipe," *Proceedings of International Conference on Offshore Mechanics and Engineering 2001*, Rio De Janeiro, Brazil, (2001), paper number MAT-3422.
4. M. Erdelen-Peppler, et al., "Can Additional Tests of HAZ Improve the Safety of Pipelines Operation?" *Science and Engineering of Gas Industry*, 1 (2009), 106 – 111.
5. BS 7448:2005 Standard: Fracture Mechanics Toughness Tests. Part 1: Method for the Determination of K_{IC} , Critical CTOD and Critical J Values of Metallic Materials, (London, UK: British Standards Institution, 2005).
6. BS 7448:2005 Standard: Fracture Mechanics Toughness Tests. Part 2: Method for the Determination of K_{IC} , Critical CTOD and Critical J Values of Welds in Metallic Materials, (London, UK: British Standards Institution, 2005).
7. E.S. Folias, "A Finite Line Crack in a Pressured Cylindrical Sheet," *International Journal of Fracture Mechanics*, (1965), 104–113.

8. BS 7910:1999 Standard: Guide on Methods for Assessing the Acceptability of Flaws in Fusion Welded Structures. Annex G: The Assessment of Corrosion in Pipes and Pressure Vessels, (London, UK: British Standards Institution, 2005).
9. D. Pumpyansky, et al., "Crack Propagation and Arrest in X70 1420 x 21.6 Pipes for New Gas Transportation System," *Proceedings of International Pipeline Conference 2008*, Calgary, Canada, (2008), paper number IPC2008-64474.
10. Y. Morozov, L. Efron, and S. Nastich, "The Main Directions of Development of Pipe Steels and Large Diameter Pipe Production in Russia," *Proceedings of International Pipeline Technology Conference 2009*, Oostende, Belgium, (2009), 1649-1658.
11. J. Wolodko, M. Stephans, "Applicability of Existing Models for Predicting Ductile Fracture Arrest in High Pressure Pipelines," *Proceedings of ASME International Pipeline Conference 2006*, Calgary, Canada (2006), paper number 10110.
12. G.M. Wilkovsky, et al., "Effect of Grade on Ductile Fracture Arrest Criteria for Gas Pipelines," *Proceedings of ASME International Pipeline Conference 2006*, Calgary, Canada (2006), paper number 10350.
13. G. Re, et al., "Recommendation for Arrest Toughness for High Strength Pipeline Steels," *3R International*, 34 (10/11) (October/November 1995).
14. V. Pistone and G. Mannucci, "Fracture Arrest Criteria for Spiral Welded Pipes," *Proceedings of the 3rd International Pipeline Conference 2000*, ed. R. Denys, Elsevier Scientific, 1 (2000), 455 – 467.
15. G. Knauf, "Crack Arrest and Girth Weld Acceptance for Pressure Gas Transmission Pipelines," *Proceedings of International Conference Evaluation and Application of High Grade Linepipes in Hostile Environments 2002*, Japan, Yokohama, (2002), 475-500.

